

Turing instability-induced oscillations in coupled reaction-diffusion systems

Nan Wang(王楠), Yuan Tong(仝源), Fucheng Liu(刘富成), Xiaoxuan Li(李晓璇), Yafeng He(贺亚峰), and Weili Fan(范伟丽)

Citation: Chin. Phys. B, 2025, 34 (**3**): 038201. DOI: 10.1088/1674-1056/ada42b
Journal homepage: http://cpb.iphy.ac.cn; http://iopscience.iop.org/cpb

What follows is a list of articles you may be interested in

Unpinning the spiral waves by using parameter waves

Lu Peng(彭璐) and Jun Tang(唐军)
Chin. Phys. B, 2021, 30 (**5**): 058202. DOI: 10.1088/1674-1056/abd46e

Exploring the role of inhibitory coupling in duplex networks

Cui-Yun Yang(杨翠云), Guo-Ning Tang(唐国宁), Hai-Ying Liu(刘海英)
Chin. Phys. B, 2017, 26 (**8**): 088201. DOI: 10.1088/1674-1056/26/8/088201

Numerical simulation and analysis of complex patterns in a two-layer coupled reaction diffusion system

Li Xin-Zheng (李新政), Bai Zhan-Guo (白占国), Li Yan (李燕), He Ya-Feng (贺亚峰), Zhao Kun (赵昆)
Chin. Phys. B, 2015, 24 (**4**): 048201. DOI: 10.1088/1674-1056/24/4/048201

Effect of metal oxide arrester on the chaotic oscillations in the voltage transformer with nonlinear core loss model using chaos theory

Hamid Reza Abbasi, Ahmad Gholami, Seyyed Hamid Fathi, Ataollah Abbasi
Chin. Phys. B, 2014, 23 (**1**): 018201. DOI: 10.1088/1674-1056/23/1/018201

The influence of long-range links on spiral waves and its application for control

Qian Yu (钱郁)
Chin. Phys. B, 2012, 21 (**8**): 088201. DOI: 10.1088/1674-1056/21/8/088201

Turing instability-induced oscillations in coupled reaction–diffusion systems

Nan Wang(王楠)[1], Yuan Tong(仝源)[1], Fucheng Liu(刘富成)[1,†], Xiaoxuan Li(李晓璇)[1], Yafeng He(贺亚峰)[1], and Weili Fan(范伟丽)[1,2,‡]

[1] *College of Physics Science and Technology, Hebei University, Baoding* 071002, *China*
[2] *Hebei Province Research Center for Basic Disciplines of Computational Physics, Baoding* 071002, *China*

(Received 21 July 2024; revised manuscript received 22 December 2024; accepted manuscript online 31 December 2024)

A new type of localized oscillatory pattern is presented in a two-layer coupled reaction–diffusion system under conditions in which no Hopf instability can be discerned in either layer. The transitions from stationary patterns to asynchronous and synchronous oscillatory patterns are obtained. A novel method based on decomposing coupled systems into two associated subsystems has been proposed to elucidate the mechanism of formation of oscillating patterns. Linear stability analysis of the associated subsystems reveals that the Turing pattern in one layer induces the other layer locally, undergoes a supercritical Hopf bifurcation and gives rise to localized oscillations. It is found that the sizes and positions of oscillations are determined by the spatial distribution of the Turing patterns. When the size is large, localized traveling waves such as spirals and targets emerge. These results may be useful for deeper understanding of pattern formation in complex systems, particularly multilayered systems.

Keywords: oscillations, localized oscillatory pattern, Turing instability, coupled reaction–diffusion system

PACS: 82.40.Ck, 47.54.–r, 82.40.Bj, 05.65.+b

DOI: 10.1088/1674-1056/ada42b **CSTR:** 32038.14.CPB.ada42b

1. Introduction

Pattern formation is ubiquitous in a remarkable variety of natural and living systems, from chemical reactions to living cells to environmental patterns.[1–6] It is well known that symmetry-breaking bifurcations of a homogeneous state are responsible for the emergence of spatiotemporal patterns.[7] Generally, the primary oscillatory (Hopf bifurcation or wave) bifurcation breaks the temporal symmetry of a system and gives rise to oscillations, while the stationary (Turing) bifurcation breaks the spatial symmetry and generates stationary spatial periodic patterns.[8,9] A combination of oscillatory and stationary bifurcations gives rise to various oscillatory Turing patterns.[10–15]

Recently, attention has turned toward oscillations in spatially extended systems in which neither Hopf nor wave instabilities of homogeneous states are present.[16–24] These oscillations may arise from secondary instabilities of nonuniform states or other mechanisms that the standard linear stability analysis cannot discern. For instance, Aragon *et al*. revealed that a series of secondary bifurcations of Turing patterns caused by nonlinear effects could generate time oscillations and chaos in the Barrio–Varea–Aragon–Maini model.[16] Ward and Wei emphasized that the Hopf bifurcation of spike solutions is also responsible for the emergence of oscillations.[17] Recently, it was demonstrated that cross diffusion is able to induce a subharmonic destabilization of the fundamental subcritical Turing mode and leads to complex dynamic behaviors, including out-of-phase oscillatory Turing patterns.[18,19] Vanag and Epstein reported a new type of out-of-phase oscillation in a spatially extended bistable system with no oscillatory instabilities.[20] More recently, Krause *et al.*[23] stated that oscillatory behavior could also be caused by the destabilization of a steady spike pattern induced by a simple spatial heterogeneity.

Coupled systems, as a special variation of classical reaction–diffusion systems, have received broad attention not only from the perspective of fundamental theory but also for their vast applications in many fields of physics, biology, ecology, networks and other sciences.[25–29] In the past two decades, a variety of oscillatory patterns have been found in coupled systems, arising from interactions of two or more different instabilities including Turing–Hopf instabilities[30] or Turing-wave instabilities.[31] Moreover, it is surprising that oscillatory patterns can also be obtained from the interaction of Turing–Turing instabilities in both linearly and nonlinearly coupled reaction–diffusion systems.[32–34] Coupling-induced rhythmogenesis may be responsible for the emergence of these oscillations.[32]

Here we report a new type of localized oscillatory pattern induced by Turing instability in a reaction–diffusion system with two coupled layers, one of which supports Turing pat-

†Corresponding author. E-mail: hdlfc@hbu.edu.cn
‡Corresponding author. E-mail: fanweili@hbu.edu.cn

© 2025 Chinese Physical Society and IOP Publishing Ltd. All rights, including for text and data mining, AI training, and similar technologies, are reserved.

terns while the other exhibits homogeneous steady states. A novel method based on decoupling coupled systems into separate subsystems that influence each other has been proposed to elucidate the mechanism of formation of these oscillating patterns.

2. Model description

To explore the mechanism of formation of oscillations in coupled reaction–diffusion systems with no Hopf bifurcation in either layer we begin with two identical coupled layers, each of which can be described by a two-component reaction–diffusion Brusselator model. The two-layer coupled model is governed by the following set of equations:

$$\begin{aligned}
\Sigma_1:&\begin{cases}\frac{\partial u_1}{\partial t}=f_1(u_1,v_1)+\alpha(u_2-u_1)+D_{u_1}\nabla^2 u_1,\\ \frac{\partial v_1}{\partial t}=g_1(u_1,v_1)+D_{v_1}\nabla^2 v_1,\end{cases}\\
\Sigma_2:&\begin{cases}\frac{\partial u_2}{\partial t}=f_2(u_2,v_2)+\alpha(u_1-u_2)+D_{u_2}\nabla^2 u_2,\\ \frac{\partial v_2}{\partial t}=g_2(u_2,v_2)+D_{v_2}\nabla^2 v_2,\end{cases}
\end{aligned} \tag{1}$$

where u and v refer to the dimensionless concentrations of the activator and inhibitor in layer 1 (Σ_1) and layer 2 (Σ_2), D_u and D_v denote the corresponding diffusion coefficients of species u and v, respectively, and α is the coupling strength of vertical diffusion between these two layers. The functions $f$and g specifying the kinetic behavior of the Brusselator model are given by

$$\begin{cases} f_{1,2}(u,v)=a-(b_{1,2}+1)u+u^2v,\\ g_{1,2}(u,v)=b_{1,2}u-u^2v,\end{cases} \tag{2}$$

where a and b are the control parameters determining the local dynamics of the system. The coupled system (1) has only one homogeneous steady state $(u_{10},v_{10,},u_{20},v_{20})=(a,b_1/a,a,b_2/a)$. The linear stability of this homogeneous steady state can be calculated from the equation

$$\left|\boldsymbol{A}-\boldsymbol{D}k^2-\lambda\boldsymbol{I}\right|=0,$$

where $\boldsymbol{A}$ is the Jacobian matrix and $\boldsymbol{D}$ is the diffusion matrix. The Hopf bifurcation line [$\mathrm{Im}(\lambda)\neq 0$, $\mathrm{Re}(\lambda)=0$ at $k=0$] and the Turing bifurcation line [$\mathrm{Im}(\lambda)\neq 0$, $\mathrm{Re}(\lambda)=0$ at $k\neq 0$] intersect at a two codimension–two bifurcation point. These two bifurcation lines separate the parametric space into four distinct regions: the stable steady state region, the pure oscillatory (Osc) region, the pure Turing region, and the oscillatory–Turing (Osc-Turing) region, in which both Hopf and Turing instabilities occur. Unless specified otherwise, the parameters are chosen as $a=3$, $b_1=9.4$, $b_2=9.5$, $D_{u_1}=D_{v_1}=8.33$, $D_{u_2}=46.0$, $D_{v_2}=120.0$ and $\alpha=0.4$.

Figure 1(a) shows the bifurcation diagram for individual layers deduced from the standard linear stability analysis. It is noticeable that layer 1 locates in the steady state region while layer 2 is in the Turing region. In order to avoid Turing instability in layer 1, we set $D_{u_1}=D_{v_1}=D_1$ throughout this paper. The dispersion curve of the coupled system (1) is illustrated in Fig. 1(b). Since the real part of the most positive eigenvalue $\mathrm{Re}(\lambda)<0$ at $k=0$, no Hopf bifurcations is present. Similarly, wave instability also does not exist. There is an unstable Turing band with the most unstable mode located at $(k_\mathrm{T},h_\mathrm{T})$. Here $k_\mathrm{T}=0.215$ is the wave number of the Turing mode (the most unstable mode), and its corresponding real part of the eigenvalue $h_\mathrm{T}=0.345$ stands for the linear growth rate of the Turing mode.

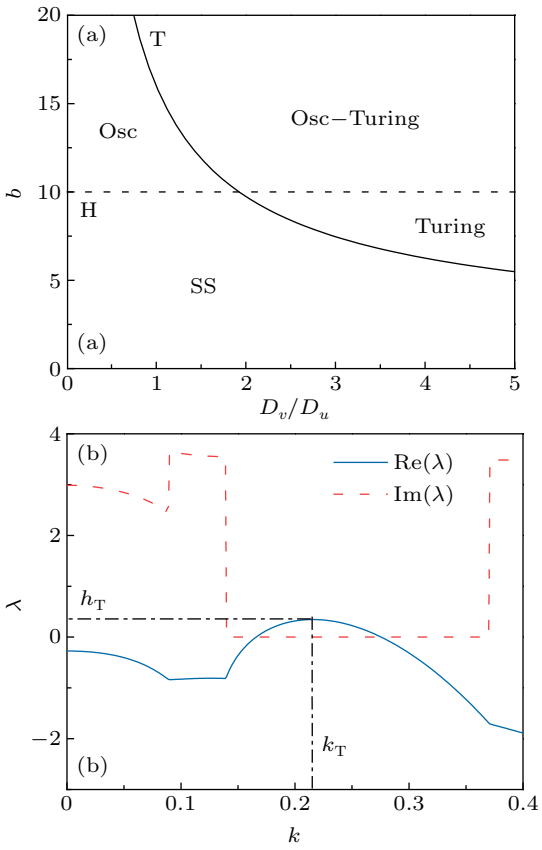


Fig. 1. Phase diagram for individual layers (a) and dispersion relation curve for coupled system (1) with $\alpha=0.4$ (b). In (a), the solid and dashed lines stand for the Turing (T) and Hopf (H) bifurcation curves, respectively. In (b), the solid and dashed lines stand for the real part and imaginary part of eigenvalues, respectively. Other parameters are $a=3$, $b_1=9.4$, $b_2=9.5$, $D_1=8.33$, $D_{u_2}=46.0$ and $D_{v_2}=120.0$.

3. Results and discussion

In all our simulations, equation (1) is integrated on a square lattice with 256×256 space units by utilizing the Peaceman–Rachford variant of the alternating direction implicit method[35] with periodic boundary conditions. A grid spacing of one unit and a time step of 0.01 are used and similar results are obtained with smaller grid spacings and time steps. A random perturbation drawn from a normal distribution with mean 0 and standard deviation 1 is added to the uniform steady state as the initial conditions. In order to ensure the stability of

simulation results, the integration time of all simulation results in this paper exceeds 2000 time units.

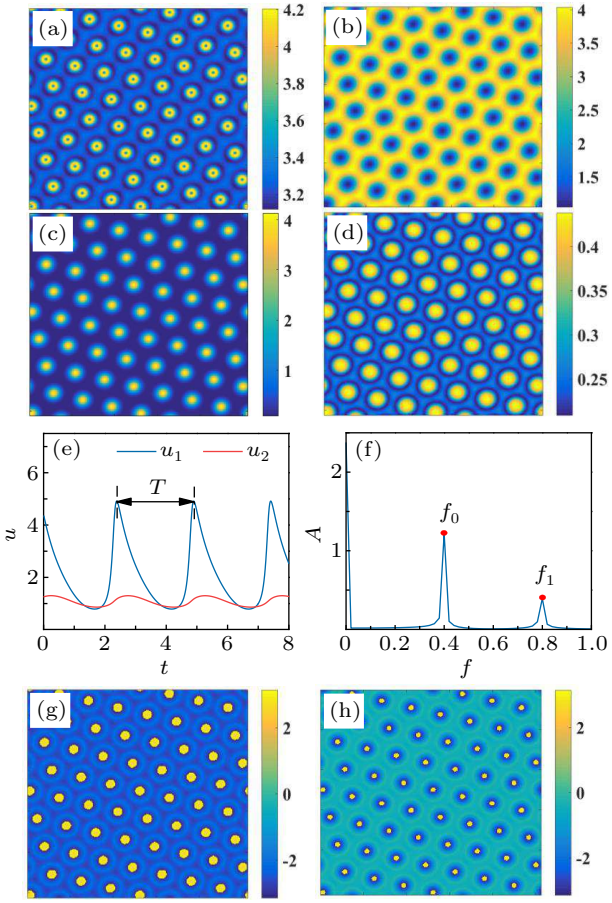


Fig. 2. Oscillatory hexagonal patterns in the coupled system (1). Panels (a) and (b) are snapshots of activators (u_1 and u_2) in layer 1 and layer 2, respectively; (c) and (d) are the corresponding amplitude distributions of oscillatory hexagonal patterns in (a) and (b). (e) Time variation of u_1 and u_2 at the center of any spot in a hexagonal pattern. (f) The Fourier spectrum of time variation of u_1 at the center of an arbitrary spot a in hexagonal pattern. (g) Phase distribution diagram of the harmonic mode with frequency $f_0 = 0.4$. (h) Phase distribution diagram of the higher harmonic mode with frequency $f_1 = 2f_0$. The parameters are the same as those in Fig. 1(a).

Figure 2 shows the simulated oscillatory hexagonal patterns in the coupled system. All the points in both layers are oscillating with the same period $T = 2.52$ but different amplitudes, giving rise to different appearances of the patterns in different layers. Generally, layer 1 exhibits a spot hexagonal pattern while layer 2 exhibits a honeycomb hexagonal pattern, as shown in Figs. 2(a) and 2(b), respectively. It should be noted that the corresponding patterns are steady state and stationary stripe patterns when these two layers are uncoupled. Figures 2(c) and 2(d) give the corresponding spatial distributions of oscillating amplitudes. The amplitude in layer 1 is much larger than in layer 2. It manifests as a hexagonal lattice with the intrinsic wave number $k_1 = 0.19$, which is slightly lower than the most unstable Turing mode $k_T = 0.215$ predicted by the linear stability analysis in Fig. 1(a). The amplitude peaks are located at the center of the spots in the hexagonal pattern, which also corresponds to the valley center of the honeycomb pattern in layer 2. This implies that the oscillating amplitude of u_1 is inversely related to the concentration of activator u_2. Figure 2(e) gives an example of oscillations at the center of an arbitrary spot in the hexagonal pattern. Obviously, u_2 are oscillating synchronously with the same period as u_1 but at a small amplitude. There is also a small phase lag, which implies that oscillations of u_2 should be attributed to the oscillations of u_1. Figure 2(f) shows the power spectrum of the time series of u_1 in Fig. 2(e). The fundamental mode with frequency $f_0 = 0.4$ and its harmonic mode $f_1 = 2f_0$ emerges, giving rise to relaxation-type oscillations. Moreover, the phase distributions of these two modes are demonstrated in Figs. 2(g) and 2(h), respectively. It can be seen that they both exhibit white-eye-like patterns with an abrupt phase between central spots and their surrounding rings. This pattern resembles the mixed mode pattern in the vicinity of the codimension-2 Turing–Hopf point in reaction–diffusion systems.[36]

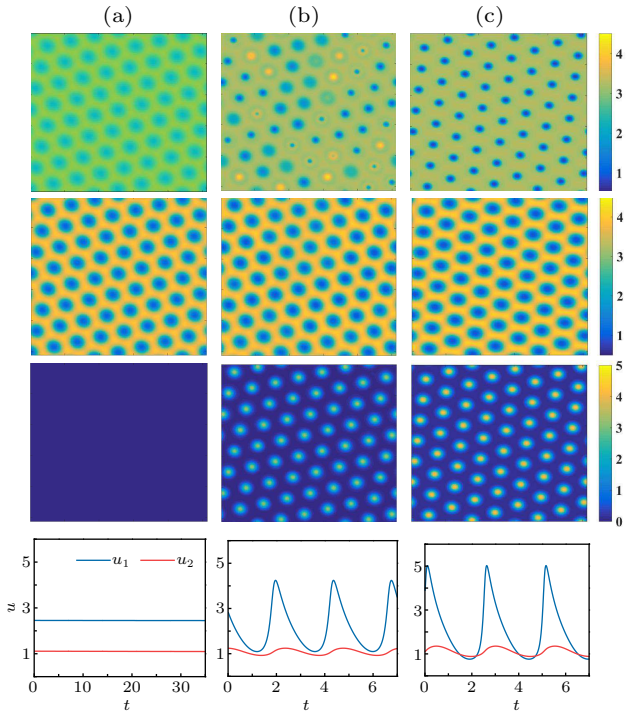


Fig. 3. Transition from static to oscillatory hexagonal patterns with increasing b_1: (a) static hexagonal pattern, $b_1 = 7$; (b) asynchronous oscillating hexagonal pattern, $b_1 = 9.2$; (c) synchronous oscillating hexagonal pattern, $b_1 = 9.5$. The panels from top to bottom show snapshots of u_1 and u_2, the corresponding amplitude distributions of u_1, and time series of u_1 and u_2 at the center of an arbitrary spot, respectively. Other parameters are the same as those in Fig. 1(a).

The parameter b_1 in layer 1 plays an important role in the formation of the oscillatory patterns. Figure 3 shows the transition from static hexagonal patterns to oscillatory hexagonal patterns as parameter b_1 is increased. At $b_1 = 7$, layer 1 exhibits the same static honeycomb hexagonal pattern as layer 2, as shown in Fig. 3(a). When b_1 is increased to a critical value $b_c = 8.8$, the valleys of the honeycomb pattern become unstable and oscillations emerge at these positions. Near the onset, these oscillations are out of phase with each other and result

in an asynchronous oscillating hexagonal pattern (Fig. 3(b)). However, as b_1 increases far above onset, all oscillations are in phase and a synchronous oscillating hexagonal pattern appears, as shown in Fig. 3(c). No matter whether the oscillating hexagonal pattern is synchronous or not, its amplitude distribution exhibits a simple pattern with spots arranged in a hexagonal lattice. The maximum amplitude is located at the core of each spot.

In Fig. 4, we present the angular frequency $\omega = 2\pi/T$ and the maximum amplitude $A_{\max}$ of oscillations in layer 1 as functions of b_1. For convenience, we introduce $\varepsilon = b_1 - b_c$ as the distance exceeding a critical value. It is obvious that the angular frequency ω is in a linear relationship with ε, which satisfies $\omega = 2.9 - 0.5\varepsilon$. At onset $\varepsilon = 0$, the frequency approximately equal to characteristic frequency $\omega_0 = a$ is close to Hopf bifurcation. This behavior is reminiscent of bulk oscillations induced by supercritical Hopf bifurcation.[7,37] The dependence of the maximum amplitude value $A_{\max}$ on ε can be represented as $A_{\max} = 5.96\sqrt{\varepsilon + 0.148} - 1.1$. It is slightly different from that of bulk oscillations, whose amplitude is proportional to $\sqrt{\varepsilon}$.[7] This discrepancy can be interpreted by the effects of lateral diffusion and inter-layer coupling. Considering that the Brusselator model always has a supercritical Hopf bifurcation,[38] it is reasonable to speculate that the formation of these oscillations can be attributed to the presence of local Hopf bifurcation in the region with a lower concentration of u_2. In this sense, the oscillatory hexagonal pattern in layer 1 can be regarded as local oscillations induced by the Turing pattern in layer 2, while oscillating Turing patterns with small amplitude in layer 2 are caused by coupling-induced rhythmogenesis.

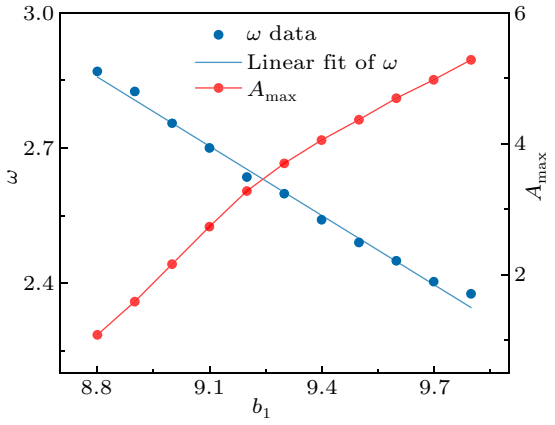


Fig. 4. The period and the maximum amplitude of oscillatory hexagonal pattern in layer 1 as a function of b_1. The parameters are the same as those in Fig. 3.

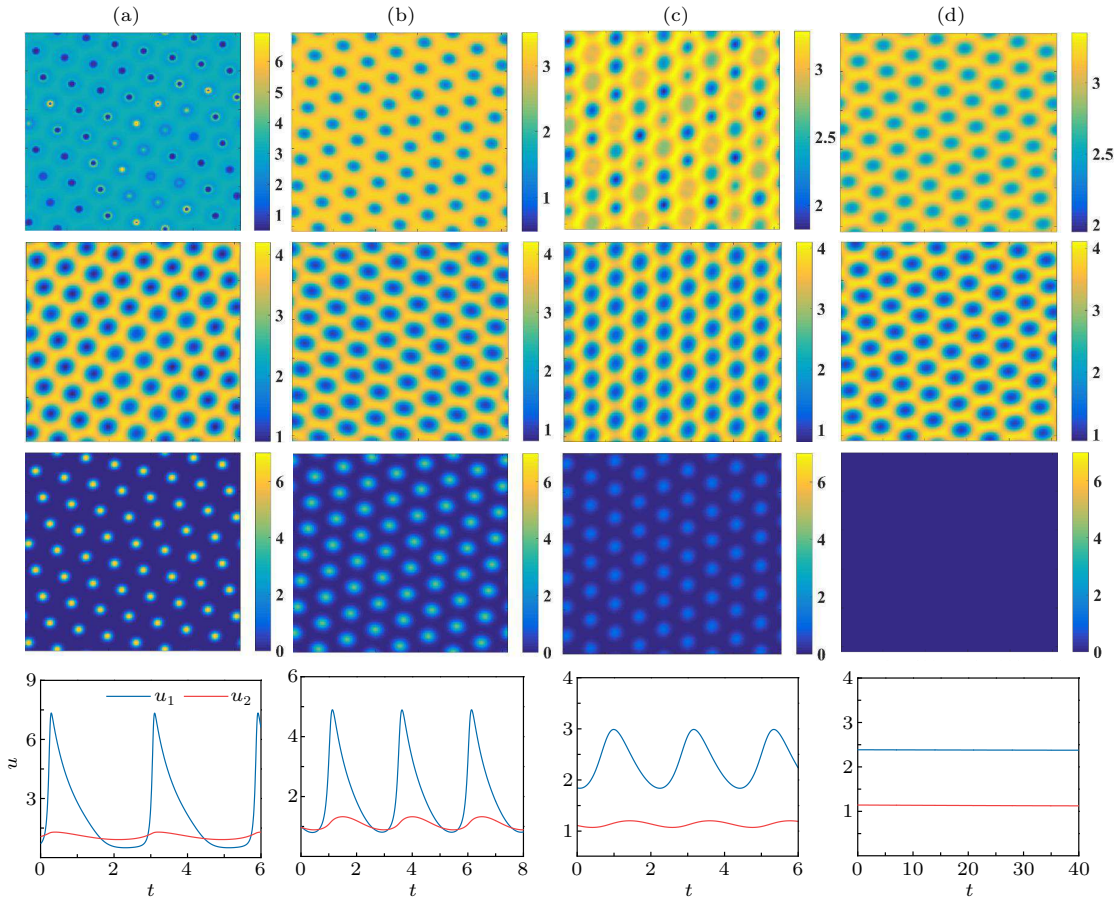


Fig. 5. Transition from oscillating to static hexagonal patterns with increasing D_1: (a) asynchronous hexagonal pattern, $D_1 = 1.6$; (b) synchronous hexagonal pattern, $D_1 = 8.0$; (c) twinkling hexagonal pattern, $D_1 = 13.5$; (d) static hexagonal pattern, $D_1 = 20.0$. The panels from up to bottom show snapshots of u_1, and u_2, the corresponding amplitude distributions of u_1, and time series of u_1 and u_2 at the center of an arbitrary spot, respectively. Other parameters are $a = 3$, $b_1 = 9.4$, $b_2 = 9.5$, $D_{u_2} = 46.0$, $D_{v_2} = 120.0$ and $\alpha = 0.4$.

Note that these localized oscillations separated by surrounding non-oscillating regions interact with each other via the diffusion process, and the diffusion coefficient has a significant impact on the characteristics of these oscillations. Figure 5 illustrates the effect of diffusion coefficient D_1 on the resulting patterns. It exhibits a transition from oscillating patterns to a stationary pattern with increasing D_1. When the diffusion is small enough (e.g., $D_1 = 1.6$), the interaction between the localized oscillations is so weak that each localized oscillation oscillates independently and an asynchronous hexagonal pattern appears, as shown in Fig. 5(a). As D_1 is increased, this asynchronous hexagonal pattern first evolves into a synchronous hexagonal pattern (Fig. 5(b)) and then into a twinkling hexagonal pattern (Fig. 5(c)) in which three subgroups oscillate with phase difference $2\pi/3$. Similar twinkling-eye patterns have been reported in both uncoupled and coupled reaction–diffusion systems.[30,31,36] Note that each oscillation is surrounded by a non-oscillating region; the interaction between oscillations and their background is increased as well with the increase of D_1, this makes the amplitude of oscillations become smaller and smaller. The maximum amplitude $A_{\max}$ and angular frequency ω of oscillations in layer 1 as functions of diffusion coefficient D_1 are depicted in Fig. 6. The maximum amplitude is $A_{\max} = 3.8\sqrt{14.72-\varepsilon} - 13.89$, while the angular frequency is $\omega = 2.88 - 0.045\varepsilon$. In this case, the distance is defined as $\varepsilon = D_c - D_1$, where $D_c = 16$ stands for the critical value for onset of oscillation. When the diffusion coefficient D_1 is larger than D_c, the oscillations disappear and a stationary hexagonal pattern forms, as demonstrated in Fig. 5(d). It is worth noting that D_c is positively correlated with the diffusion coefficients in layer 2. To spontaneously form oscillatory patterns, the diffusion coefficients in layer 1 must be much smaller than those in layer 2.

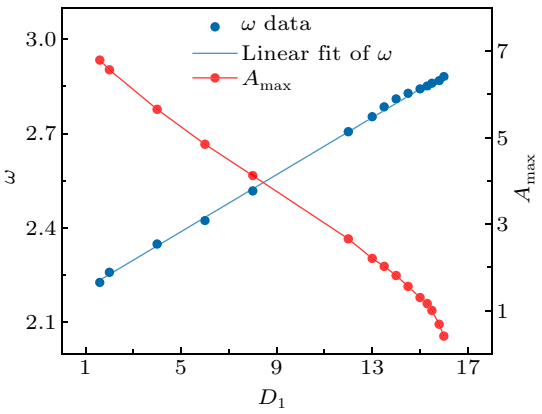


Fig. 6. The period and the maximum amplitude of oscillating hexagonal patterns in layer 1 as functions of D_1. Other parameters are the same as those in Fig. 5.

In order to gain further insight into the relation between synchronization and pattern formation, we calculate the synchronization factor by using mean field theory, which is written as[39–41]

$$\begin{cases} F = \frac{1}{N^2}\sum_{j=1}^{N}\sum_{i=1}^{N} x_{i,j}, \\ R = \frac{\langle F^2\rangle - \langle F\rangle^2}{\frac{1}{N^2}\sum_{j=1}^{N}\sum_{i=1}^{N}\left(\langle x_{i,j}^2\rangle - \langle x_{i,j}\rangle^2\right)}, \end{cases} \tag{3}$$

where N is number of nodes of the system and x is the system variable. The symbol $\langle * \rangle$ represents the average value of the variable over time.

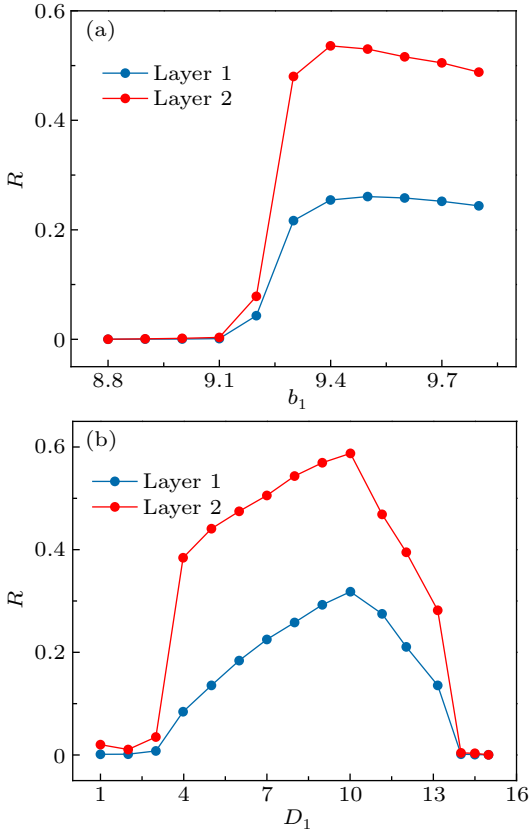


Fig. 7. (a) and (b) The relationship between the synchronization factor R vs. b_1 and D_1, respectively.

The dependence of the synchronization factors R for each layer on the tunable parameters b_1 and D_1 is shown in Figs. 7(a) and 7(b), respectively. As depicted in Fig. 7(a), it is obvious that the synchronization factor takes a value around 0 near the onset, indicating non-synchronization. All the oscillations are out of phase with each other in this case. The synchronization factor R gradually increases when the parameter b_1 is increased to 9.1 and reaches the maximum at $b_1 = 9.4$. In this situation, all oscillations are in phase and a synchronous oscillating hexagonal pattern appears. With further increase in b_1, the synchronization factor R will decrease slightly. The reason for this decrease may be attributed to the emergence of the Hopf mode as the system moves towards the Hopf bifurcation point $b_c^H = 1 + a^2 = 10$. It should be noted that the synchronization factor R in layer 2 is always larger than that in layer 1. Comparing Fig. 7(b) with Fig. 5, one can see that

the parameter region where a synchronous oscillating hexagonal pattern appears is nearly the same region in which the synchronization factor R has a relatively large value. When D_1 is small enough, the lateral diffusion is too weak to support synchronization, resulting in the synchronization factor R decreasing gradually to a value around zero. However, when D_1 is large, the synchronization factor R also decreases dramatically to zero due to the attenuation of oscillations.

The hypothesis put forward for the origin of localized oscillations in a hexagonal pattern can be verified by analyzing the dynamics of layer 1 while adding an external term proportional to the Turing pattern from layer 2. Intuitively, the two-layer coupled system (1) can be viewed as two associated subsystems, each of which behaves as an external environment. In this sense, each subsystem in coupled system (1) can be rewritten as

$$\begin{cases} \frac{\partial u}{\partial t} = a-(b+1)u+u^2v+\alpha(u'-u)+D_u\nabla^2 u, \\ \frac{\partial v}{\partial t} = bu-u^2v+D_v\nabla^2 v, \end{cases} \tag{4}$$

where the notation is the same as in Eq. (1) while u' is the concentration of activator in the other subsystem (layer). Strictly speaking, system (4) should be viewed as a spatially heterogeneous reaction–diffusion system with heterogeneous steady-state states. Therefore, linear stability analysis at a heterogeneous steady-state state should be carried out. However, the standard procedure of stability analysis is not easily extendable to the case with a heterogeneous steady state. A recent advance in the study of pattern formation in spatially heterogeneous reaction–diffusion systems was made in Refs. [42,43]. Unfortunately, the exact function of the spatially dependent coefficient u' could not be obtained because it is coupled with the other subsystems. Therefore, as a first step, we treat the coefficient u' as a constant in the local region, and perform the stability analysis of the homogeneous steady state $(u_0,v_0)=((a+\alpha u')/(1+\alpha),b(1+\alpha)/(a+\alpha u'))$ of this subsystem. It goes through a Hopf bifurcation if $b>b_{\rm c}^{\rm H}=1+\alpha+u_0^2$, evolving then into a bulk oscillation characterized by an intrinsic frequency $\omega_0=a$. The steady state may also undergo a Turing bifurcation when $b>b_{\rm c}^{\rm T}=\left[\sqrt{1+\alpha}+u_0\sqrt{D_u/D_v}\right]^2$, giving rise to a stationary spatial pattern with an intrinsic wave number $k_{\rm T}$.

For $a=3$ and $\alpha=0.4$, the critical value $b_{\rm c}^{\rm H}$ for onset of Hopf bifurcation as a function of u' is shown in Fig. 8. The smaller u' is, the smaller $b_{\rm c}^{\rm H}$ is. As far as subsystem 1 (layer 1) is concerned, $u'=u_2(x,y)$ determines the local critical value $b_{\rm c}^{\rm H}$, and vice versa. That is, the sizes and positions of oscillations are determined by the spatial distribution of the Turing pattern $u'=u_2(x,y)$. Taking the oscillating hexagonal pattern in Fig. 2 ($b=9.4$ here) as an example, the corresponding value for the onset $b_{\rm c}^{\rm H}=9.4$ is $u'=2.4$. Consequently, in the region where $u'(x,y)$ is lower than 2.4, the subsystem 1 undergoes Hopf bifurcation and gives rise to oscillations. In other words, oscillations arise in the region where u_2 is lower than 2.4 in layer 2, as depicted in Fig. 2(b). If b is small enough, the corresponding value of u' is too low to be achieved in layer 2, so no oscillation takes place. This is the case in Fig. 3(a), where the critical value $u'=0.8$ for $b=7$ is lower than the minimum of u_2 in layer 2. It should be emphasized that the localized oscillations here are essentially different from those in systems arising from subcritical Hopf or wave instabilities, in which appropriate initial conditions must be satisfied.[14,15]

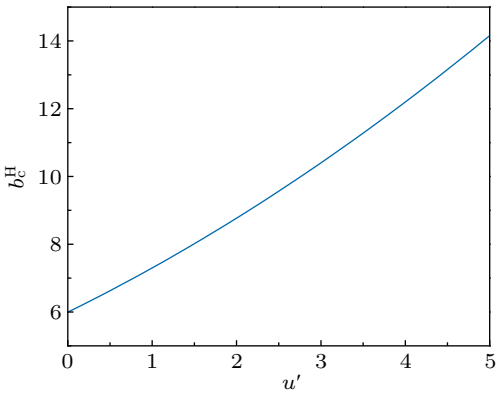


Fig. 8. The linear stability analysis of homogeneous state $(u_0,v_0)=((a+\alpha u')/(1+\alpha),b(1+\alpha)/(a+\alpha u'))$ in two-variable reaction–diffusion systems with a source described by Eq. (2). The critical value for Hopf bifurcation $a=3$, $b_{\rm c}^{\rm H}=1+\alpha+u_0^2$, $\alpha=0.4$.

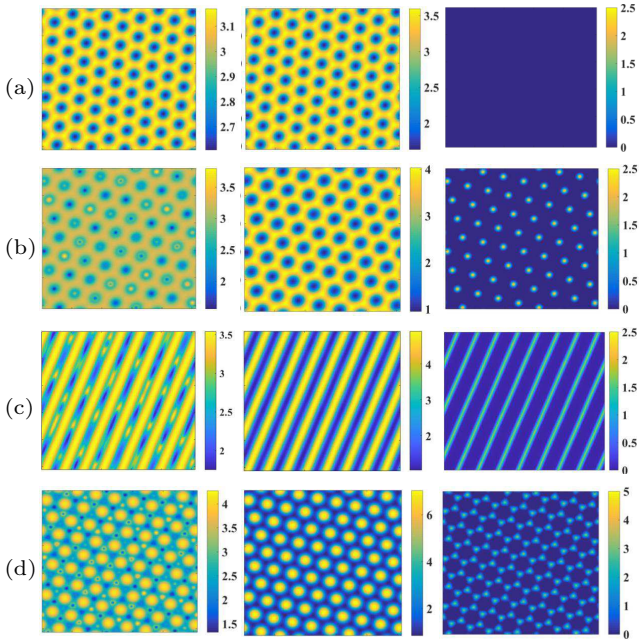


Fig. 9. Effect of Turing structures on localized oscillations: (a) static honeycomb hexagonal pattern, $D_{v_2}=110$; (b) oscillating honeycomb hexagonal pattern, $D_{v_2}=123$; (c) oscillating stripe pattern, $D_{v_2}=145$; (d) oscillating spot hexagonal pattern, $D_{v_2}=240$. The first column shows a snapshot of u_1, the middle column is a snapshot of u_2, and the last column is the corresponding amplitude distribution of u_1. Other parameters are $a=3$, $b_1=7.9$, $b_2=9.5$, $D_1=1$, $D_{u_2}=46.0$ and $\alpha=0.4$.

Depending on the spatial configuration and magnitude of Turing patterns in layer 2, various localized oscillating pat-

terns can be obtained. Figure 9 gives several examples of localized oscillating patterns in layer 1. Here the Turing pattern is varied by the diffusion coefficient D_{v_2} while keeping other parameters unchanged. At $D_{v_2} = 110$, the growth rate of the Turing mode is small ($h_{\mathrm{T}} = 0.312$). Hence, the amplitude of the Turing patterns is too small to make the minimum of u_2 lower than the critical value u', resulting in the absence of local Hopf bifurcation. In this situation, a Turing hexagonal pattern appears in both layers, as shown in Fig. 9(a). As D_{v_2} is increased, the growth rate as well as the amplitude of the Turing mode increase gradually. When the minimum of u_2 reaches the critical value u', localized oscillations form and the system exhibits localized oscillating patterns, including the honeycomb hexagonal pattern, stripe pattern and spot hexagonal pattern, as shown in Figs. 9(b)–9(d) respectively.

The frequency and maximum amplitude of these oscillating patterns as functions of D_v are given in Fig. 10. On varying the control parameter D_{v_2} the sequence honeycomb hexagons (region I) $\rightarrow$ honeycomb hexagon–stripe mixture (region II) $\rightarrow$ stripes (region III) $\rightarrow$spot hexagon–stripe mixture (region IV) $\rightarrow$ spot hexagons (region V) is observed. The pattern selection of Turing patterns in layer 2 is responsible for the transition between these oscillating patterns. The same sequence of Turing patterns has been observed both numerically and theoretically in the classical two-variable Brusselator model as the control parameter is increased.[44,45] For mixture patterns in region 2, a few localized oscillations are embedded in a stationary stripe pattern (not shown here). For each oscillating pattern, there is a negative correlation between its angular frequency ω and its maximum amplitude $A_{\max}$.

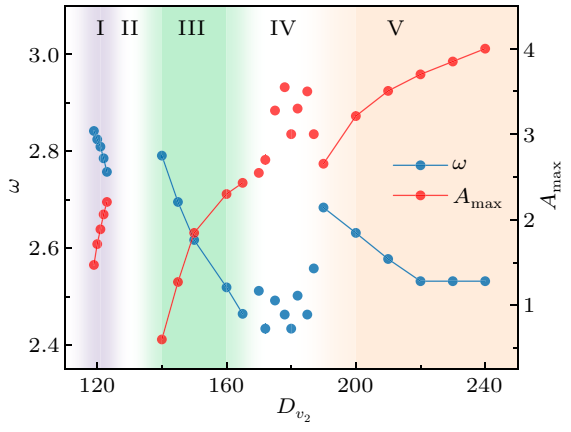


Fig. 10. The period and the maximum amplitude of the oscillating pattern in layer 1 as a function of D_{v_2}. The parameters are the same as those in Fig. 9.

The size of each localized oscillating region in an oscillating pattern is proportional to the wavelength $\lambda = 2\pi/k_{\mathrm{T}}$ of the Turing patterns. If the size is large, traveling waves can be formed in the localized oscillating region. Figure 11 gives an example of isolated spirals or target waves arranged on a hexagonal lattice. In each local region there is a localized spiral wave or target wave, as shown in Fig. 11(a). From the amplitude distributions in Fig. 11(b), one can see that the core of the spiral wave is a topological defect whose amplitude is zero. This isolated spiral pattern is remarkably similar to that in the two-layer coupled reaction–diffusion model induced by wave instability.[31] This indicates that the same patterns may originate from different mechanisms.

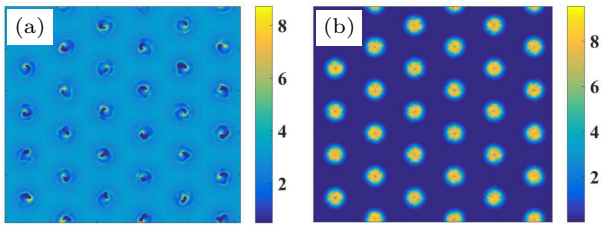


Fig. 11. Isolated spirals or targets on a hexagonal array of Turing spots: (a) snapshot of activator (u_1) in layer 1; (b) the corresponding amplitude distribution. Parameters are $a = 3$, $b_1 = 9.4$, $b_2 = 9.5$, $D_1 = 0.5$, $D_{u_2} = 110$, $D_{v_2} = 260.87$ and $\alpha = 0.4$.

4. Conclusion

In summary, a novel type of localized oscillatory pattern is reported in a reaction–diffusion system with two coupled layers, one of which supports Turing patterns while the other exhibits homogeneous steady states. Contrary to the localized structures arising from subcritical instabilities in which a necessary finite amplitude localized perturbation is required, the localized oscillatory pattern here is attributed to a supercritical Hopf bifurcation occurring in the local region where the concentration of Turing patterns in the other layer is below a critical value. A novel approach by decomposing coupled systems into separate subsystems is proposed to analyze theoretically the underlying mechanism of pattern formation in coupled systems via standard linear analysis. The predicted results are in good agreement with numerical simulations. This work provides a step towards a deeper understanding the formation of spatiotemporal patterns in multilayered systems and other complex systems.

Acknowledgments

Project supported by the National Natural Science Foundation of China (Grant Nos. 12275065, 12275064, and 12475203), the Natural Science Foundation of Hebei Province (Grant Nos. A2021201010 and A2024201020), Interdisciplinary Research Program of Natural Science of Hebei University (Grant No. DXK202108), Hebei Provincial Central Government Guiding Local Science and Technology Development Funds (Grant No. 236Z1501G), Scientific Research and Innovation Team Foundation of Hebei University (Grant No. IT2023B03), and the Excellent Youth Research Innovation Team of Hebei University (Grant No. QNTD202402).

References

[1] Cross M and Greenside H 2009 *Pattern Formation and Dynamics in Non-Equilibrium Systems* (New York: Cambridge University Press)
[2] Xu H R and Wu Y L 2024 *Nature* **627** 553
[3] Liu Y, Chen D, Tian J, Xu W and Jiao Y 2024 *Phys. Rev. Lett* **133** 028401
[4] Gante H F 2018 *Science* **362** 396
[5] Echeverria-Alar S, Pinto-Ramos D and Tlidi M C M G 2023 *Phys. Rev. E* **107** 054219
[6] Sun Y, Wang J, Li Y, Jiang N and Xia J 2023 *Chin. Phys. B* **32** 090203
[7] Cross M C and Hohenberg P C 1993 *Rev. Mod. Phys.* **65** 851
[8] Yang L F, Zhabotinsky A M and Epstein I R 2004 *Phys. Rev. Lett.* **92** 198303
[9] Turing A M 1952 *Bulletin of Mathematical Biology* **237** 37
[10] Wit A D, Lima D, Dewel G and Borckmans P 1996 *Phys. Rev. E* **54** 261
[11] Yang L F, Dolnik M, Zhabotinsky A M and Epstein I R 2002 *The Journal of Chemical Physics* **117** 7259
[12] Ledesma-Durán A and Aragón J L 2019 *Chaos, Solitons and Fractals* **124** 68
[13] Ledesma-Durán A and Aragón J L 2019 *Sci. Rep.* **9** 11287
[14] Li Y and Zhou Y 2023 *Chaos, Solitons and Fractals* **171** 113473
[15] Vanag V K and Epstein I R 2004 *Phys. Rev. Lett.* **92** 128301
[16] Aragón J L, Barrio R A, Woolley T E, Baker R E and Maini P K 2012 *Phys. Rev. E* **86** 26201
[17] Ward M J and Wei J 2003 *Journal of Nonlinear Science* **13** 209
[18] Gambino G, Lombardo M C and Sammartino M 2018 *Phys. Rev. E* **97** 012220
[19] Li A W, Jin Z, Li L and Wang J Z 2012 *Int. J. Mod. Phys. B* **26** 1250193
[20] Vanag V K and Epstein I R 2005 *Phys. Rev. E* **71** 066212
[21] Painter K J and Hillen T 2011 *Phys. D* **240** 363
[22] Page K M, Maini P K and Monk N A M 2005 *Phys. D* **202** 95
[23] Krause A L, Klika V, Woolley T E and Gaffney E A 2018 *Phys. Rev. E* **97** 052206
[24] Catlla A J, McNamara A and Topaz C M 2012 *Phys. Rev. E* **85** 026215
[25] Pal K, Paul S and Ray D S 2020 *Phys. Rev. E.* **101** 052203
[26] Fan W, Ma F, Tong Y, Liu Q, Liu R, He Y and Liu F 2023 *Physical Chemistry Chemical Physics* **25** 26023
[27] Barrio R A, Baker R E, Vaughan B, Tribuzy K, De Carvalho M R, Bassanezi R and Maini P K 2009 *Phys. Rev. E* **79** 031908
[28] Wang W and Liu S T 2023 *New J. Phys.* **25** 023008
[29] Konishi K, Yoshida K, Sugitani Y and Hara N 2024 *Phys. Rev. E* **109** 014220
[30] Yang L, Dolnik M, Zhabotinsky A M and Epstein I R 2002 *Phys. Rev. Lett.* **88** 208303
[31] Yang L F and Epstein I R 2003 *Phys. Rev. Lett.* **90** 178303
[32] Ji L and Li Q S 2006 *Chem. Phys. Lett.* **424** 432
[33] Liu Y, Dong M F, Liu F C, Tian M, Wang S and Fan W 2021 *Acta. Phys. Sin.* **70** 158201 (in Chinese)
[34] Kytta K, Kaski K and Barrio R A 2007 *Phys. A* **385** 105
[35] Sgura I, Bozzini B and Lacitignola D 2012 *Journal of Computational and Applied Mathematics* **236** 4132
[36] Sarría-González J, Sgura I and Ricard M R 2021 *International Journal of Bifurcation and Chaos* **31** 2150164
[37] Aranson I S and Kramer L 2002 *Rev. Mod. Phys.* **74** 99
[38] Zemskov E P, Vanag V K and Epstein I R 2011 *Phys. Rev. E* **84** 036216
[39] Gonze D, Bernard Y S, Waltermann C, Kramer A and Herzel H 2005 *Biophysical Journal* **89** 120
[40] Ma J and Tang J 2017 *Nonlinear Dynam.* **89** 1569
[41] Wang X, Du J, Li Z, Ma M and Li C 2024 *Acta Phys. Sin.* **73** 110503 (in Chinese)
[42] Krause A L, Václav K, Woolley T E and Gaffney E A 2020 *Journal of The Royal Society Interface* **17** 20190621
[43] Calderón-Barreto E A, Castillero J B and Aragón J L 2024 *Chaos, Solitons and Fractals* **179** 114433
[44] Verdasca J, Wit A D, Dewel G and Borckmans P 1992 *Phys. Lett. A* **168** 194
[45] Peña B and Pérez-García C 2001 *Phys. Rev. E* **64** 056213